Spectrochimica Acta Part A: Molecular and Biomolecular Spectroscopy 128 (2014) 724–729

Contents lists available at ScienceDirect

Spectrochimica Acta Part A: Molecular and Biomolecular Spectroscopy

journal homepage: www.elsevier.com/locate/saa

# Synthesis, spectral and quantum chemical studies on NO-chelating sulfamonomethoxine–cyclophosph(V)azane and its Er(III) complex

Abdel-Nasser M.A. Alaghaz [a,b,*], Reda A.A. Ammar [c], Gottfried Koehler [d], Karl Peter Wolschann [e], Tarek M. El-Gogary [f,*]

[a] Department of Chemistry, Faculty of Science (Boys), Al-Azhar University, Nasr City, Cairo, Egypt
[b] Department of Chemistry, Faculty of Science, Jazan University, Jazan, Saudi Arabia
[c] Department of Chemistry, King Saud University, P.O. Box 2455, Riyadh 11451, Saudi Arabia
[d] Max F Perutz Laboratories, University of Vienna, 1030 Vienna, Austria
[e] Institute for Theoretical Chemistry, University of Vienna, 1090 Vienna, Austria
[f] Department of Chemistry, Faculty of Science, Damietta University, Damietta, Egypt

## HIGHLIGHTS

- A novel cyclodiphosph(V)azane ligand, was synthesized and characterized by different tools.
- Quantum chemical calculations were used to support the measured results.
- Geometry optimization was performed at the level of B3LYP/6-31G(d).
- Simulated IR and UV–VIS spectra showed agreement with the measured values.
- Reactivity of the title compound was discussed in terms of accommodation of charge and HOMO picture.

## GRAPHICAL ABSTRACT

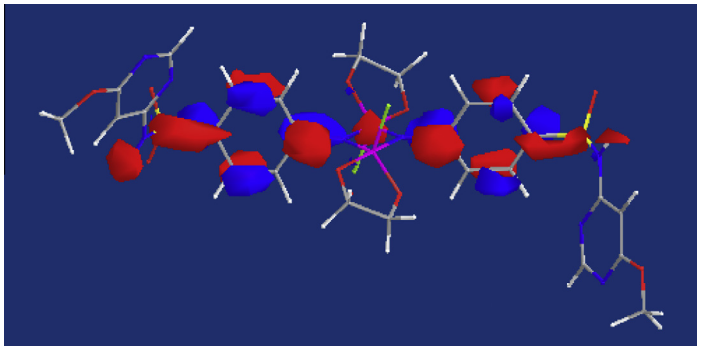

## ARTICLE INFO

*Article history:*
Received 18 October 2013
Received in revised form 10 February 2014
Accepted 13 February 2014
Available online 27 February 2014

*Keywords:*
Cyclodiphosph(V)azane
Sulfamonomethoxine erbium(III) complex
B3LYP
TD–DFT

## ABSTRACT

Computational studies have been carried out at the DFT-B3LYP/6-31G(d) level of theory on the structural and spectroscopic properties of novel ethane-1,2-diol-dichlorocyclophosph(V)azane of sulfamonomethoxine (L), and its binuclear Er(III) complex. Different tautomers of the ligand were optimized at the *ab initio* DFT level. Keto-form structure is about 15.8 kcal/mol more stable than the enol form (taking zpe correction into account). Simulated IR frequencies were scaled and compared with that experimentally measured. TD–DFT method was used to compute the UV–VIS spectra which show good agreement with measured electronic spectra. The structures of the novel isolated products are proposed based on elemental analyses, IR, UV–VIS, $^{1}$H NMR, $^{31}$P NMR, SEM, XRD spectra, effective magnetic susceptibility measurements and thermogravimetric analysis (TGA).



* Corresponding authors. Address: Department of Chemistry, Faculty of Science (Boys), Al-Azhar University, Nasr City, Cairo, Egypt (A.-N.M.A. Alaghaz). Tel.: +966 500972289 (T.M. El-Gogary).
*E-mail address:* tarekelgogary@yahoo.com (T.M. El-Gogary).

http://dx.doi.org/10.1016/j.saa.2014.02.061
1386-1425/

## Introduction

In recent years, the structural feature of four-membered $P_2N_2$ ring compounds in which the coordination number of P varies from three to five have attracted considerable attention [1,2]. Heterocycles with P—C, P—N, P—O, and P—S bonds, in addition to their great biochemical and commercial importance [3,4], play a major role in some substitution mechanisms heterocycles had been found to be potentially carcinostatics [3] among other pharmacological activities. The introduction of tervalent P centers in the ring enhanced the versatility of the heterocycles in complexing with both hard and soft metals. Since the tervalent P centers could stabilize transition metals in low oxidation states [3,4], such complexes could be potential homogeneous or phase-transfer catalysts in various organic transformations [3]. There is considerable current interest in compounds containing spiro and ansa organic P rings [5]. Although the ammonolysis of some 1,3-diaryl-2,4-dichlorocyclodiphosph(V)azans had been investigated in some detail, little was known about the interaction of hexachlorocyclodiphosph(V)azanes with bifunctional reagents. The reaction of bifunctional reagents with cyclodiphosph(V)azanes could give rise in principle to four types of structures named spiro, ansa, cross-linking, and only one functionality attached, while the other remains free. Spiro, ansa, and cross linking structures of phosphazanes were now well studied synthetically, spectroscopically, and crystallographically [5]. The reaction of hexachlorocyclodiphosph(V)azanes with amino compounds, active-methylene-containing compounds, and bifunctional reagents had been investigated in some details [6,7]. Sulfonamides were the oldest class of antimicrobials and were still the drug of choice for many diseases such as cancer and tuberculosis [8]. Cyclophosphamide and its derivatives were examples of phosphorus compounds which were one of the most effective anticancer agents with proven activity against a large variety of human cancers [9]. Hexachlorocyclodiphosph(V)azanes of sulfonamides and their complexes had been prepared [6,10–13]. In continuation to our interest to prepare hexachlorocyclodiphosph(V)azane of sulfa drugs [14,15], the present paper aims chiefly to prepare ethane-1,2–diol-dichlorocyclodiphosph(V)azane L. The behavior of this ligand toward erbium(III) ion was studied. The characterization of the prepared compounds was performed using different physicochemical methods.

## Experimental

Melting points (°C, uncorrected) were determined in open capillaries on a Gallen Kemp melting point apparatus. Elemental analysis (C, H, N and S) were performed on Carlo Erba 1108 Elemental Analyzer. The chlorine content was determined by the Schöninger method, phosphorus content was determined by the vanadomolybdato–phosphoric acid spectrophotometric method and water molecules were determined by the thermogravimetric analysis. Analysis of the erbium complex started with decomposition of the complex with concentrated nitric acid. The resultant solution was diluted with distilled water, filtered to remove the precipitated ligand. The solution was then neutralized with aqueous ammonia solution and the metal ions titrated with EDTA. The infrared spectra were recorded on a Shimadzu FT-IR spectrometer using KBr disks. Electronic spectra were recorded for solution of the ligand, L in DMF, and for the metal complexes as Nujel Mull on a Jasco UV–VIS spectrophotometer model V-550-UV–VIS. $^1$H NMR spectra (in $CDCl_3$) were recorded on Bruker Ac-300 ultrashield NMR spectrometer at 300 MHz, using TMS as internal standard. $^{31}$P NMR spectra were run, relative to external $H_3PO_4$ (85%), with a Varian FT-80 spectrometer at 36.5 MHz. The mass spectrum of L ligand was performed using a Shimadzu-Ge–Ms–Qp 100 EX mass spectrometer using the direct inlet system. The molar conductance measurements were carried out using a Sybron–Barnstead conductometer. Magnetic susceptibilities were measured at room temperature using the Faraday method with a Cahn–Ventron RM-2 balance standardized with $HgCo(NCS)_4$; diamagnetic corrections were estimated from Pascal's constants. Thermogravimetric analysis was performed under a nitrogen atmosphere using a Shimadzu TGA-50H with a flow rate of 20 ml min$^{-1}$.

### *Synthesis of L ligand*

1,3-bis(N$^1$-4-amino-6-methoxypyrimidinebenzenesulfonamide)-2,2,2,4,4,4-hexachlorocyclodiphosph(V)azane(0.1 mol, 83.1 g) in 100 ml cold dry benzene was added in small portions to a well stirred cold solution of ethan-1,2-diol (0.2 mol, 12.4 g) in 100 ml cold dry benzene during half an hour at ≈15 °C under dry conditions. After completion of the reaction (HCl gas ceased to evolve), filtration and removal of all solvent in vacuo, a residue was obtained which on crystallization (Fig. 1).

**L:** White solid, Yield, 81%; m.p. 126 °C. Molar conductance ($\Lambda_M$): 1.14 $\Omega^{-1}$ cm$^2$ mol$^{-1}$. Anal. calcd. for $C_{30}H_{32}Cl_2N_4O_{10}P_2S_2$ (M.Wt. 805.58): C, 44.73; H, 4.00; Cl, 8.80; N, 6.95; O, P, 7.69; S, 7.96. Found: C, 44.25; H, 3.86; Cl, 8.43; N, 6.41; P, 7.60; S, 7.78.

$^1$H NMR ($CDCl_3$) (300 MHZ, 298 K); $\delta$ = 6.73 (2H, t, aromatic, $J_1$ = 8.4 HZ, $J_2$ = 10.8 HZ), 6.95 (2H, d, aromatic $J$ = 8.1 HZ), 6.95 (2H, d, aromatic, $J$ = 7.4 HZ), 7.32 (2H, t, aromatic $J_1$ = 8.4 HZ, $J_2$ = 6.8 HZ), 7.36 (1H, d, $J$ = 8.21 Hz), 7.13 (1H, d, $J$ = 8.52 Hz), 5.12 (2H, s, —$SO_2$NH), 3.72 (6H, s, —$OCH_3$), 3.66 (8H, s, —O—$CH_2$).

### *Synthesis of erbium complex*

The erbium complex was prepared by adding dropwise hot aqueous (60 °C) solution (100 ml) of $ErCl_3{\cdot}6H_2O$ (0.76 g; 0.002 mol) to a solution of L (0.805 g; 0.001 mol) in tetrahydrofuran (THF) (20 ml) while stirring continuously. After complete addition of the $ErCl_3{\cdot}6H_2O$ solution, the reaction mixture was heated under reflux for about 28 h under dry conditions. The complex obtained was filtered, washed with water, ethanol, and THF and then dried in vacuo (Fig. 2).

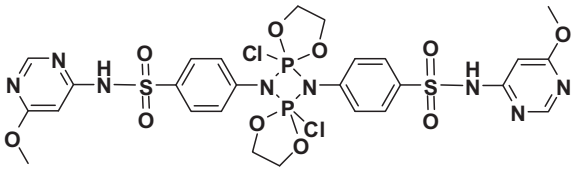

**Fig. 1.** Proposed structure of L ligand.

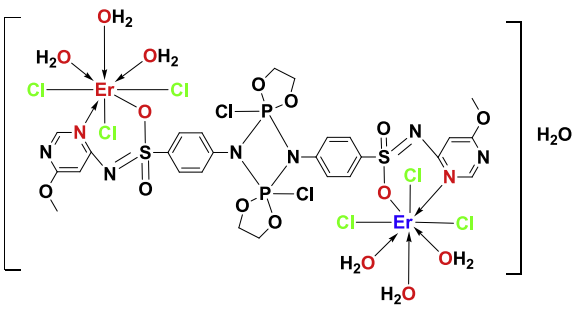

**Fig. 2.** Suggested structure of erbium-L binuclear complex.

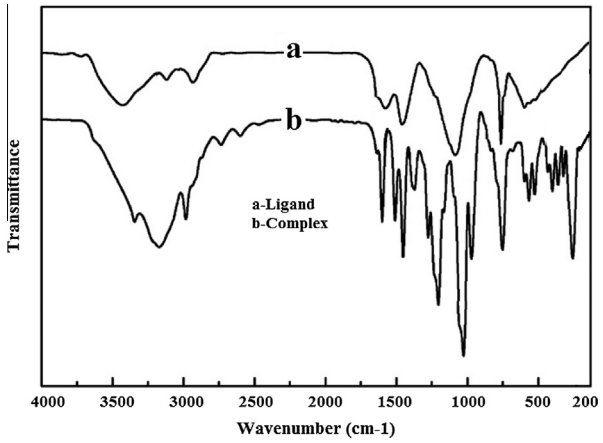


**Fig. 3.** IR spectrum of (a) ligand (L) and (b) Er(III) complex.

*$[Er_2(L)(H_2O)_6Cl_6]H_2O$:* Pink solid, Yield, 73%; m.p. 198 °C: Molar conductance ($\Lambda_M$): 2.24 $\Omega^{-1}$ $cm^2$ $mol^{-1}$. Anal. calcd. for $C_{26}H_{42}Cl_8Er_2N_8O_{17}P_2S_2$.

*(M.Wt. 1482.87):* C, 21.06; H, 2.85; Cl, 19.13; Er, 22.56; N, 7.56; P, 4.18; S, 4.32. Found: C, 20.98; H, 2.47; Cl, 19.02; Er, 22.48; N, 7.33; P, 4.11; S, 4.24.

## Computational methods

All quantum chemical calculations were performed using the Gaussian09 suite of programs [16]. Geometry optimization of the ligand have been performed using the *ab initio* Density Functional Theory (DFT) at the B3LYP functional [17–19] in conjunction with the 6-31G(d) basis set. For each stationary point, we carried out a force constant harmonic frequency calculation at the same levels to characterize their nature as minima or transition states and to correct energies for zero-point energy and thermal contribution. The frequencies are scaled by a factor of 0.98. The vibrational modes were animated using the ChemCraft program [20]. Natural charges were computed within full Natural Bond Orbital analysis, using NBO program implemented in Gaussian 09 [16]. Erbium binuclear complex was optimized at B3LYP/UGBS1P [21] for the erbium atoms and 6-31G(d) for other atoms of the complex.

## Results and discussion

### *Experimental studies*

The L structure is unambiguously assigned by $^1$H NMR (Fig. S1), $^{13}$C NMR (Fig. S2), $^{31}$P NMR (Fig. S3), and FTIR (Fig. 3). The $^1$H NMR spectrum (Fig. S1) of the ligand L revealed its formation by the presence of —NH proton signal at $\delta$ = 5.12 ppm. This is further supported by the appearance of stretching vibration band $\nu$(NH) imine at 3365 $cm^{-1}$. Also, the $^1$H NMR of the ligand exhibits signals at $\delta$(ppm) = 3.66 (s, 6H, $2OCH_3$) and 9.82 (br, 2H, —OH, exchangeable with $D_2O$). This is an experimental evidence for the tautomerization. The $^{13}$C NMR spectrum shows an obvious peak of the carbon of C—P on the ligand at 47.62 ppm, the carbon of —$CH_3$ and —$CH_2$- appears in 16.34 and 62.87 ppm, respectively. The $^{31}$P NMR spectrum shows a strong singlet at 24.96 ppm, indicating that the two phosphorus groups in the molecule have the same chemical environment.

The IR data are listed in Table 1. The $SO_2$ group modes of the ligand appear as medium to small bands at 1345 $cm^{-1}$ ($\nu_{asym}$) and 1083 $cm^{-1}$ ($\nu_{sym}$) for L ligand. In the complex, the asymmetric and symmetric modes are shifted to 1324 $cm^{-1}$ and 1099 $cm^{-1}$for the asymmetric and symmetric modes, respectively, upon coordination

**Table 1**
Characteristic IR bands of the ligand (L) and its $[Er_2(L)(H_2O)_6Cl_6]H_2O$ complex as KBr pellets.

| Assignments | L | $[Er_2(L)(H_2O)_6Cl_6]H_2O$ |
|---|---|---|
| $\nu_{asym}(SO_2)$ | 1346s | 1325s |
| $\nu_{sym}$ $(SO_2)$ | 1084s | 1090s |
| $\nu$(NH) | 3366br | 3370br |
| $\nu(CH)_{aromatic}$ | 3024m | 3024m |
| $\nu(CH)_{aliphatic}$ | 2937m | 2936m |
| $\nu$(C═N) | 1622m | 1557m |
| $\rho r(H_2O)$ | – | 824s |
| $\rho w(H_2O)$ | – | 775s |
| $\nu$(M—O) | – | 489s |
| $\nu$(M—N) | – | 422s |
| $\nu$(M—Cl) | – | 486m |
| $\nu(P—N)_{cyclic}$ | 1225m | 1225m |
| $\nu(P—N)_{linear}$ | 1005m | 984m |
| $\nu$(P—Cl) | 586m | 584m |
| $\nu$(P—O—C) | 1114m | 1116m |
| $\nu$(P—N—P) | 1014m | 990w |
| $\nu$(N—P—N) | 816m | 813m |

to the metal ion [22]. The stretching vibration band; $\nu$(NH), of the sulfonamide group, which found at 3365 $cm^{-1}$ in the free ligand, were shifted to higher frequencies in the spectra of the isolated complex. The presence of coordinated water molecules renders it difficult to confirm the enolization of the sulfonamide group. The blue shift of the $SO_2$ stretching vibration to lower frequencies may be attributed to the transformation of the sulfonamide to the enol form as a result of complex formation to give a more stable six-membered ring [14,15]. This transformation would result in the loss of the amide proton and the appearance of the absorption peak for enol $\nu$(OH) stretching mode at 2923 $cm^{-1}$ for the complex, together with a change in position and intensities of the sulfone group [14,15]. This is supported by the $^1$H NMR data. The enolic OH group is formed through the following tautomerism [15,22,23].

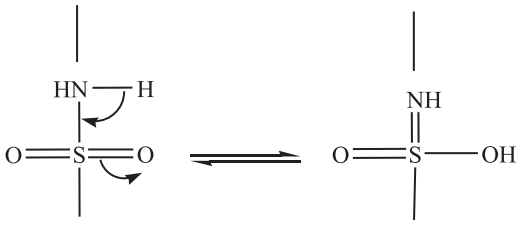


The lower frequencies of the enolic OH groups can be taken as evidence for the participation of this group in complex formation [14,15]. The strong and sharp bands at 1621 $cm^{-1}$ of the pyrimidine-N; $\nu$(C═N) in the free ligand is shifted to 1595 $cm^{-1}$ in the erbium complex. This indicates the participation of the pyrimidine-N in complex formation [14,15]. The presence of medium-to-strong bands in the region between 816 and 765 $cm^{-1}$ in the spectrum of the erbium complexes were attributed to coordinated water molecules [14,15]. New bands were found in the spectrum of the complex in the regions 488 and 421 $cm^{-1}$ which were assigned to $\nu$(M—O) and $\nu$(M—N) stretching vibrations, respectively [14,15].

Therefore, the IR data reveal that L ligand behaves as neutral bidentate ligand and bind to the metal ion through enolic sulfonamide OH and pyrimidine-N.

The UV spectrum (Fig. 4) of the ligand in DMF solvent showed absorption band at 276 nm, which are due to the electron delocalization within the four membered ring of the dimeric structure for the ligand [14,15].

### *Computational studies*

Since single crystal X-ray structure for the novel hexachlorocyclophosph(V)azane of sulfamonomethoxine ligand is not

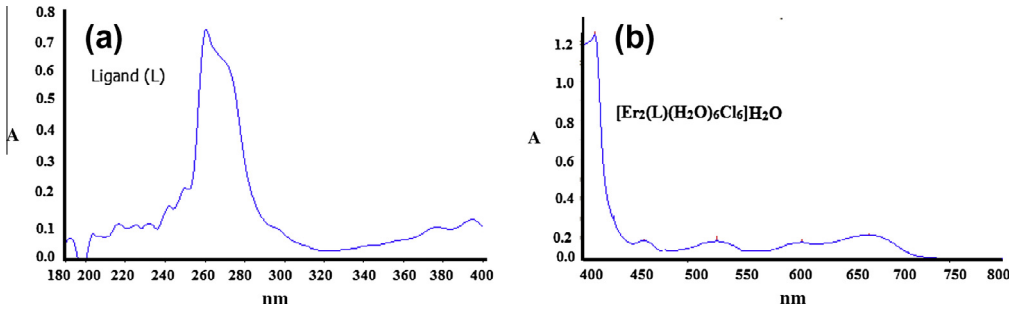


**Fig. 4.** Electronic spectrum of (a) ligand (L) and (b) Er(III) complex.

available, quantum chemical calculations were utilized to find the geometry optimized structures for the L at B3LYP/6-31G(d) quantum mechanical method. Fig. S4 shows the optimized structure of the L at B3LYP/6-31G(d). An inspection of the resulting structure easily shows two close contacts H-bonding interactions. Table S1 in the supplementary material presents computed geometrical parameters of L. Although the system is big-sized (46 non-hydrogenic atoms) the optimization process goes smoothly till reached a local minimum after 29 steps as shown in Figs. S5 and S6. Figs. S7 and S8 in the supplementary material present the structure of the ligand L, showing the atom symbols and atomic numeration respectively. Since dispersion energies do not play a considerable role in these types of structure, electron correlations are not so important consequently DFT methods would provide a good quality structures. The $P_2N_2$ ring is almost planar and P—N bonds in the ring are not of equal length. The average bond length is 1.754 Å. The P—Cl bond length is 2.089 Å. Our structural data given in Table S1 in Supplementary material agrees well with the available X-ray data on $P_2N_2$ ring-containing compounds [23,24] and also with our previous computations [24,25] add also the new paper [24–26].

Simulated IR spectra of L were calculated at the level B3LYP/6-31G(d). Fig. 5 displays the simulated IR spectra for the keto tautomer scaled by 0.98 as a scale factor [26]. Inspection of the calculated frequencies shows that they agree with the experimentally measured IR spectra Fig. 3a and Table 1. The vibrational frequencies were animated with ChemCraft to assign frequencies to their normal modes. The C=N stretching frequency measured as a medium peak around 1620 computed as a very strong peak at 1647. The asymmetric stretching of $SO_2$ which measured around 1346 was computed at 1391 $cm^{-1}$.

The electronic spectrum of L in DMF showed absorption bands at 272 nm regions which is due to intra ligand $\pi \rightarrow \pi^*$ and $n \rightarrow \pi^*$ transitions involving molecular orbital of the pyrimidine ring. DT–DFT calculations were performed for the free ligand in the molecular gas state. The UV–VIS spectrum of L keto-form is shown in Fig. 6. The UV–VIS data as shown in Fig. 4 shows a sharp band at 233 nm.

Natural charges (Table 2) were computed within full Natural Bond Orbital analysis, using NBO implemented in Gaussian 09 [16]. Positive and negative charges are accommodated on some centers of the L molecule. Positive charges are found on S, P, H and some C atoms. The highest positive charge is found on S (2.351), and the next highest charge is found on P (2.256). On the other hand, negative charges are on N, O, Cl and some C atoms. The highest negative is found on N (−1.143). The coordination is processed from N20 (−0.541) and N32 (−0.544) which accommodate fairly negative charge. Coordination also links oxygen atoms that carry approximately (−0.900) of negative charge. The distribution of charge on the ligand accounts for the importance of the electrostatic interaction for the course of bonding with the erbium(III) metal ion upon complexation.

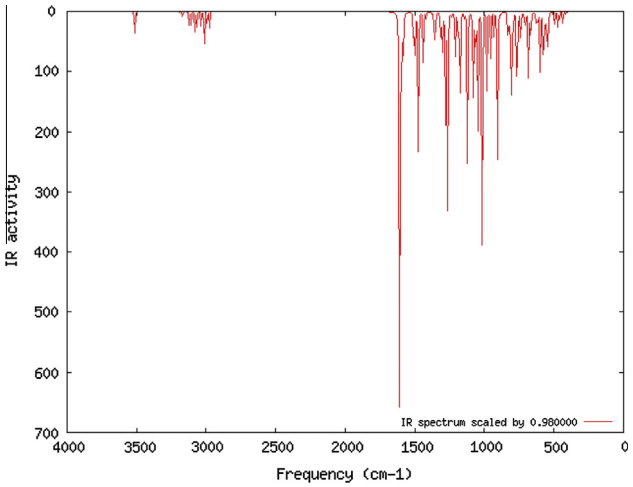


**Fig. 5.** Simulated IR spectrum of keto-form of L.

HOMO and LUMO pictures of the hexachlorocyclophosph(V)azane of sulfamonomethoxine (L) are shown in Figs. S9 and S10. HMO are located at the tail of the structure on the pyrimidine ring, and sulfamonomethoxine. This part of the molecule is interacting with the metal ions. Where this part behaves as a bidentate ligand from the OH (after tautomerization) and the pyrimidine N.

Possibility of keto-enol tautomerism has been taken into account. The enol structure was computed and optimized at the same level. The optimized enol structure is shown in Fig. S11. The keto structure is more stable than the enol form by about 16.3 kcal/mol. This difference is reduced to 15.8 kcal/mol if zero-point

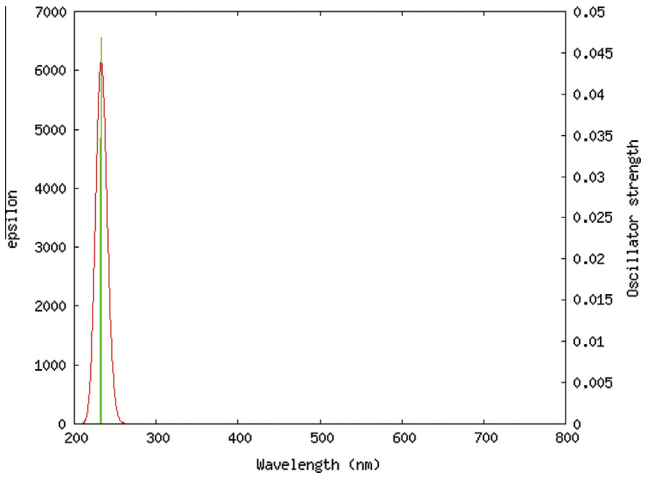


**Fig. 6.** Simulated UV–VIS spectrum of keto-form of L.

**Table 2**
Computed natural charge of all atoms in the L.

| Atom | Charge | Atom | Charge | Atom | Charge |
|---|---|---|---|---|---|
| N1 | −1.143 | C27 | −0.193 | H53 | 0.275 |
| P2 | 2.256 | C28 | −0.206 | H54 | 0.258 |
| N3 | −1.143 | S29 | 2.351 | H55 | 0.443 |
| P4 | 2.256 | N30 | −0.873 | H56 | 0.253 |
| C5 | 0.164 | C31 | 0.425 | H57 | 0.218 |
| C6 | −0.209 | N32 | −0.544 | H58 | 0.223 |
| C7 | −0.208 | C33 | −0.423 | H59 | 0.218 |
| C8 | −0.328 | C34 | 0.276 | H60 | 0.220 |
| C9 | −0.194 | N35 | −0.518 | H61 | 0.252 |
| C10 | −0.207 | C36 | 0.569 | H62 | 0.264 |
| S11 | 2.351 | O37 | −0.497 | H63 | 0.276 |
| O12 | −0.951 | C38 | −0.324 | H64 | 0.259 |
| O13 | −0.913 | O39 | −0.913 | H65 | 0.440 |
| N14 | −0.873 | O40 | −0.951 | H66 | 0.242 |
| C15 | 0.413 | Cl41 | −0.312 | H67 | 0.220 |
| C16 | −0.379 | O42 | −0.826 | H68 | 0.236 |
| C17 | 0.574 | O43 | −0.823 | H69 | 0.207 |
| N18 | −0.569 | Cl44 | −0.314 | H70 | 0.206 |
| C19 | 0.281 | O45 | −0.823 | H71 | 0.223 |
| N20 | −0.541 | O46 | −0.825 | H72 | 0.236 |
| O21 | −0.514 | C47 | −0.129 | H73 | 0.240 |
| C22 | −0.320 | C48 | −0.139 | H74 | 0.221 |
| C23 | 0.165 | C49 | −0.129 | H75 | 0.235 |
| C24 | −0.210 | C50 | −0.138 | H76 | 0.222 |
| C25 | −0.208 | H51 | 0.252 | H77 | 0.220 |
| C26 | −0.329 | H52 | 0.264 | H78 | 0.238 |

energy (zpe) correction has been taken into consideration. This large difference permits separable isomers. This allows tautomerization prior to complexation.

*Characterization of erbium(III) complex*

Er(III) complex (Fig. 4b) display five electronic spectral bands in the range of 679, 616, 527, 468, and 415 nm, characteristic to an dodecahedral geometry [27]. These bands may be assigned to the following transitions:

$^4I_{15/2} \rightarrow {}^4F_{9/2}$, $^4I_{15/2} \rightarrow {}^4S_{3/2}$, $^4I_{15/2} \rightarrow {}^2H_{11/2}$ (Er–I), $^4I_{15/2} \rightarrow {}^4F_{7/2}$, and $^4I_{15/2} \rightarrow {}^4G_{11/2}$ (Er–II), respectively. Magnetic moment of the erbium(III) complex at room temperature lie in the range 9.43 B.M. These values are in tune with a high spin configuration and show the presence of an distorted dodecahedra environment [27,28] around the Er(III) ion in the complex. This magnetic behavior of the complex indicating that the *4f* electrons in the complexes Er(III) atoms are well-shielded by the outermost *5s* and *5p* electrons. The values of the bonding parameters $\beta$ (nephelauxetic ratio), $\delta$ (Sinha's parameter) and $b^{1/2}$ (covalent factor), calculated [27,29–34] from the solid-state *f–f* spectra by Eqs. (1-3), are listed in Table 3. The values indicate that the interaction between Er(III) and the ligand is essentially electrostatic and that there is a minor participation of the *4f* orbitals in bonding [29–34].

$$\beta = \frac{1}{2}\sum_{n=1}^{n}\frac{\overline{V}\text{complex}}{\overline{V}\text{aquo}}, \quad (1)$$

**Table 3**
Bonding parameters[a,b] for the $[Er_2L(H_2O)_6Cl_6]\cdot 2H_2O$ complex.

| Compound | $\beta$ | $\delta$ | $b^{1/2}$ |
|---|---|---|---|
| $[Er_2(L)(H_2O)_6Cl_6]H_2O$ | 0.995 | +0.72 | 0.058 |

[a] Calculated from solid-state *f–f* spectra taking into account the [b]wavenumbers of the $^4I_{15/2} \rightarrow {}^4F_{9/2}$, $^4S_{3/2}$, $^2H_{11/2}$, $^4F_{7/2}$, $^4F_{5/2}$, $^4F_{3/2}$, ($^2G$, $^4F$, $^2H)_{9/2}$ and $^4G_{11/2}$ transitions.
[b] For the definition of the bonding parameters $\beta$, $\delta$ (%) and $b^{1/2}$.

$$\delta(\%) = \frac{1-\beta}{\beta} \times 100, \quad (2)$$

$$b^{1/2} = \left[\frac{1}{2}(1-\beta)^{1/2}\right]. \quad (3)$$

*Computational studies on the complex*

Erbium binuclear complex was optimized at B3LYP/UGBS1P [21] for the erbium atoms and 6-31G(d) for other atoms of the complex. Fig. S12 shows the optimized structure of the binuclear Er complex. The ligand behaves a bidentate from the enolic structure. The complex appeared in an dodecahedral structure. Coordination occurs from O and N where Er—O and Er—N bond lengths are 2.221 and 2.251 Å respectively. The Er—O of the coordinated water is a slightly longer (2.258 Å).

Fig. S13 presents the TG and derivative thermogravimetric (DTG)curves of $[Er_2(L)(H_2O)_6Cl_6]H_2O$ in nitrogen, which shows that $[Er_2(L)(H_2O)_6Cl_6]H_2O$ undergoes three-steps thermal degradation. The first decomposition step was found in the temperature range of 85–145 °C with an estimated mass loss of 1.14% (calculated mass loss of 1.21%) could be assigned to the successive loss of one hydrated water molecule. There is a slight exothermic process observed in the DTA curve from 85 to 145 °C. The second decomposition steps found within temperature range of 145–260 °C with an estimated mass loss of 7.16% (calculated mass loss 7.29%), could be assigned to the successive loss of two coordinated water molecules. The third decomposition step was found within temperature range 260–450 °C with an estimated mass loss of 63.14% (calculated mass loss 63.22%), which are reasonably accounted by the removal of the organic moieties ($C_{23}H_{26}Cl_8N_8O_7P_2S_2$), one spilt exothermic peak observed in the DTA curve at 408 °C. The decomposition of the Er(III) complex molecule ended with the metallic residue ($2Er_2O_3$) and three carbon residue with an estimated mass loss of 28.19% (calculated mass loss of 28.26%).

Fig. S14 depicts the SEM photographs of the synthesized ligand L and $[Er_2L(H_2O)_6Cl_6]H_2O$ complex. The morphology and particle size of the ligand L and $[Er_2L(H_2O)_6Cl_6]H_2O$ complex have been illustrated by the scanning electron micrography (SEM). It was noted that there is a uniform matrix of the synthesized complex in the pictograph which leads to believe that it is a homogeneous phase material. An ice fogs like shape is observed in the ligand L with the particle size of 5 μm. However $[Er_2L(H_2O)_6Cl_6]H_2O$ complex is an ice granules shaped morphology with 5 μm particle size.

Single crystal of the complex could not be prepared to get the XRD and hence the powder diffraction data was obtained for structural characterization. X-ray powder patterns of one representative complex $[Er_2(L)(H_2O)_6Cl_6]H_2O$ has been given in Fig. S15 along with the prominent data. The peak broadening at lower angle is more meaningful for the calculation of particle size; therefore the size of the particle has been calculated using Debye–Scherrer formula [35] using reflection from the XRD pattern. Debye–Scherrer formula is given by $D = 0.94\lambda/\beta Cos\,\theta$, where $D$ is the size of the particle, $\lambda$ is the wavelength of X-ray, $\beta$ is the full width at half maximum (FWHM) after correcting the instrument peak broadening ($\beta$ is expressed in radians,) and $\theta$ is the angle. The size of the particles has been found to be 33–35 nm. The size for the representative complex was obtained 16.0 nm and on this basis it could be concluded that the complex $[Er_2(L)(H_2O)_6Cl_6]H_2O$ is a nano-sized complex of erbium(III) with an dodecahedral structure. The observed X-ray pattern of the free ligand sample studied in the present investigation indicates amorphous nature.

On the basis of spectral, thermal and magnetic studies, a plausible structure for the complexes is established (Fig. 2) in which erbium(III) is situated in an dodecahedral environment.

## Conclusions

In this paper coordination chemistry of a chlorocyclodiphosph(V)azane ligand (L), obtained from the reaction of 1,3-bis($N^1$-4-amino-6-methoxypyrimidinebenzene-sulfonamide)-2,2,2,4,4,4-hexachlorocyclodiphosph(V)azane [15] and ethan-1,2-diol, is described. Binuclear erbium (III) complex of cyclodiphosph(V)-azane ligand has been synthesized and characterized on the basis of analytical, infrared, UV–VIS, $^1$HNMR, $^{13}$C NMR, $^{31}$P NMR, Mass, SEM, TEM, XRD, TGA, magnetic measurements and DFT computations. The cyclodiphosph(V)azane coordinates to the erbium ion through its enolic sulfonamide OH and pyrimidine-N. Erbium(III) complex exhibits dodecahedral geometry. Quantum chemical calculations were used to support the measured results. Geometry calculations in gas phase explored the structure of L and its erbium(III) complex. Different tautomers of the ligand were optimized at the *ab initio* DFT level. Keto-form structure is about 15.8 kcal/mol more stable than the enol form. Simulated IR and UV–VIS spectra showed agreement with the measured values. Computed natural charges shade light on the coordinating atoms as a reason of the negative charge they accommodate.

## Acknowledgment

The Authors extend their appreciation to the Deanship of Scientific Research at King Saud University for funding the work through the research group Project No. RGP-VPP-062.

## Appendix A. Supplementary material

Supplementary data associated with this article can be found, in the online version, at http://dx.doi.org/10.1016/j.saa.2014.02.061.

## References

[1] S.S. Kumaravel, S.S. Krishnamurthy, J. Chem. Soc. Dalton Trans. 1 (1990) 1119.
[2] M.S. Balakrishna, R.M. Abhyankar, J.T. Mague, J. Chem. Soc. Dalton Trans. 4 (1990) 1407.
[3] S. Priva, M.S. Balakrishna, J.T. Mague, S.M. Mobin, Inorg. Chem. 42 (2003) 1272.
[4] B. Hoge, C. Thoösen, T. Herrmann, P. Panne, I. Pantenburg, J. Fluorine Chem. 125 (2004) 831–851.
[5] A.N.M.A. Alaghaz, S.A.H. Elbohy, Phosphorus Sulfur Silicon Relat. Elem. 183 (2008) 2000.
[6] A.M.A. Alaghaz, Phosphorus Sulfur Silicon Relat. Elem. 183 (2008) 2287.
[7] A.M.A. Alaghaz, Phosphorus Sulfur Silicon Relat. Elem. 183 (2008) 2373.
[8] E.X. Esposito, K. Baran, K. Kelly, J.D. Madura, J. Mol. Graph. Model. 18 (2000) 283.
[9] M. Kel, K. Shii, Chem. Commun. 8 (2000) 669.
[10] R.A. Shaw, Phosphorus Sulfur Silicon 45 (1989) 103.
[11] M. Becke-Goehring, B.Z. Bopple, Anorg. Chem. 322 (1963) 239.
[12] A.M.A. Alaghaz, R.A. Ammar, Eur. J. Med. Chem. 45 (2010) 1314.
[13] A.M.A. Alaghaz, Phosphorus Sulfur Silicon Relat. Elem. 183 (2008) 2000.
[14] M.M. Al-Mogren, A.M.A. Alaghaz, T.M. El-Gogary, Spectrochem. Acta A 118 (2014) 481–487.
[15] M.M. Al-Mogren, A.M.A. Alaghaz, T.M. El-Gogary, S.A.H. Albohy, J. Mol. Struct. 1048 (2013) 202–209.
[16] M.J. Frisch, G.W. Trucks, H.B. Schlegel, G.E. Scuseria, M.A. Robb, J.R. Cheeseman, G. Scalmani, V. Barone, B. Mennucci, G.A. Petersson, H. Nakatsuji, M. Caricato, X. Li, H.P. Hratchian, A.F. Izmaylov, J. Bloino, G. Zheng, J.L. Sonnenberg, M. Hada, M. Ehara, K. Toyota, R. Fukuda, J. Hasegawa, M. Ishida, T. Nakajima, Y. Honda, O. Kitao, H. Nakai, T. Vreven, J.A. Montgomery, Jr., J.E. Peralta, F. Ogliaro, M. Bearpark, J.J. Heyd, E. Brothers, K.N. Kudin, V.N. Staroverov, R. Kobayashi, J. Normand, K. Raghavachari, A. Rendell, J.C. Burant, S.S. Iyengar, J. Tomasi, M. Cossi, N. Rega, J.M. Millam, M. Klene, J.E. Knox, J.B. Cross, V. Bakken, C. Adamo, J. Jaramillo, R. Gomperts, R.E. Stratmann, O. Yazyev, A.J. Austin, R. Cammi, C. Pomelli, J.W. Ochterski, R.L. Martin, K. Morokuma, V.G. Zakrzewski, G.A. Voth, P. Salvador, J.J. Dannenberg, S. Dapprich, A.D. Daniels, Ö. Farkas, J.B. Foresman, J.V. Ortiz, J. Cioslowski, D.J. Fox, Gaussian 09, Revision A.1, Gaussian Inc, Wallingford CT, 2009.
[17] A.D. Becke, J. Chem. Phys. 98 (1993) 5648.
[18] C. Lee, W. Yang, R.G. Parr, Phys. Rev. B 37 (1988) 785.
[19] P.J. Stephens, F.J. Devlin, C.F. Chabalowski, M.J. Frisch, Phys. Chem. 98 (1994) 11623.
[20] G.A. Zhurko, D.A. Zhurko, ChemCraft version 1.5, 2005.
[21] E.V.R. de Castro, F.E. Jorge, J. Chem. Phys. 108 (1998) 5225–5229.
[22] K. Nakamoto, Infrared and Raman Spectra of Inorganic and Coordination Compounds, in: Organometallic and Bioinorganic Chemistry, fifth ed., Springer, Berlin, 1997.
[23] C.M. Sharaby, G.G. Mohamed, M.M. Omar, Spectrochem. Acta (Part A) 66 (2007) 935.
[24] N.N. Bhuvan Kumar, K.C. Kumara Swamy, Polyhedron 26 (2007) 883–890.
[25] T.M. El-Gogary, A.N.M.A. Alaghaz, Reda A.A. Ammar, J. Mol. Struct. 1011 (2012) 50–58.
[26] A.M.A. Alaghaz, A.G. Al-Sehemi, T.M. El-Gogary, Spectrochim. Acta A 95 (2012) 414–422.
[27] K.A. Thiakou, V. Nastopoulos, A. Terzis, C.P. Raptopoulou, S.P. Perlepes, Polyhedron 25 (2006) 539.
[28] S. Liu, L. Gelmini, S.J. Rettig, R.C. Thompson, C. Orvig, J. Am. Chem. Soc. 114 (1992) 6081.
[29] C.K. Jorgensen, Modern Aspects of Ligand Field Theory, North-Holland, Amsterdam, 1971.
[30] S.P. Sinha, Spectrochim. Acta 22 (1966) 57.
[31] D.E. Henrie, G.R. Choppin, J. Chem. Phys. 49 (1968) 477.
[32] D.G. Karraker, Inorg. Chem. 6 (1967) 1863.
[33] D.G. Karraker, Inorg. Chem. 7 (1968) 473.
[34] A. Messimeri, C.P. Raptopoulou, V. Nastopoulos, A. Terzis, S.P. Perlepes, C. Papadimitriou, Inorg. Chim. Acta 336 (2002) 8.
[35] A. Guinier, X-ray Diffraction, San Francisco, CA, 1963.